The radial and poloidal localization of fast magnetoacoustic eigenmodes in tokamaks

T. Fülöp, M. Lisak, Ya. I. Kolesnichenko,[a] and D. Anderson
Department of Electromagnetics, Chalmers University of Technology, and Euratom–NFR Association, Göteborg, Sweden

(Received 4 October 1999; accepted 7 February 2000)

Edge-localized fast magnetoacoustic eigenmodes (FME) may be responsible for the observed superthermal ion cyclotron emission in recent deuterium/deuterium (DD) and deuterium/tritium (DT) experiments. These modes can be driven unstable by resonant interaction with a small population of energetic ions (e.g., fusion alphas), having an anisotropic distribution in velocity space, provided that the mode frequency is close to the ion cyclotron frequency. In the present paper, the radial and poloidal structure of these eigenmodes is analyzed, by solving the two-dimensional (2D) eigenmode equation both numerically and analytically using a variational approach. In particular, the conditions for the mode localization and the dependence of the mode structure on aspect ratio and ellipticity are investigated. The eigenmode is found to be radially localized near the plasma edge. In a tokamak with finite aspect ratio, the mode is localized also poloidally near the outer midplane edge. The existence of localized solutions for both sign of the poloidal mode number is found to be sensitive to the ellipticity, the magnitude of parallel wave number and the plasma density profile. © *2000 American Institute of Physics.* [S1070-664X(00)03205-5]

I. INTRODUCTION

The edge-localized fast magnetoacoustic eigenmodes (FME) are currently considered as the main candidate to explain the observed superthermal ion cyclotron emission (ICE) in recent deuterium–deuterium (DD) and deuterium–tritium (DT) experiments. When the mode frequency is close to multiples of the ion cyclotron frequency, the FME can be destabilized by resonant interaction with a subpopulation of energetic ions [fusion products, neutral beam injection (NBI) or ion cyclotron resonance heating (ICRH) produced ions], having an anisotropic distribution in velocity space near the outer edge of the plasma.

Recently, much effort has been spent on FME structure studies. Radially localized modes are important not only to explain the observed ICE, but also because these modes might open a possibility for transferring energy from the fusion products to the background ions. The first investigations were performed assuming circular cross section and infinite aspect ratio,[1,2] and suggested that the FME are radially localized in the edge region of the cylinder. More detailed studies, still in the limit of circular cross section and infinite aspect ratio,[3,4] have shown that inclusion of the Hall term affects the mode solutions and introduces a dependence on the sign of the poloidal phase velocity. In Refs. 5 and 6 the two-dimensional (2D) eigenmode equation, without the Hall term, was analyzed assuming circular cross section. The results indicated that the FME are localized both radially and poloidally close to the outer midplane edge of the tokamak. The effects of noncircular cross section, different plasma density profiles and the presence of fast ions were included in Ref. 7, in the limit of infinite aspect ratio, showing that the localization of waves of both signs of the poloidal phase velocity is possible provided that the plasma density exceeds a critical magnitude N_{cr} at the outer edge.

In the present work we perform a 2D eigenmode analysis including the symmetry breaking Hall term, the effect of elliptic cross section, finite aspect ratio ($R_0/a=3$) and finite parallel wave number, both numerically with the shooting method and analytically with a variational approach. Both methods give radially and poloidally localized eigenmodes if certain conditions are satisfied. While the radial localization is robust with respect to the inclusion of ellipticity and finite parallel wave number, the poloidal structure is more sensitive and higher order eigenmode solutions appear. Furthermore, we show that the localization of waves with both signs of the poloidal phase velocity is possible in a finite aspect ratio tokamak with high ellipticity.

The structure of the paper is the following: In Sec. II the 2D equation of the FME is derived. In Sec. III, the eigenmode equation is analyzed with a variational approach. Section IV is devoted to the numerical analysis of the eigenmode equation. Finally, in Sec. V we summarize our results.

II. THE EIGENMODE EQUATION

We consider fast magnetoacoustic waves with small parallel wave vector ($k_{\|} \ll k_{\perp}$) and with the wave frequency in the range $\omega_{ci}^2 \ll \omega^2 \ll \omega_{ce}^2$, where ω_{ci} and ω_{ce} are the ion and electron cyclotron frequencies, respectively. The eigenmode equation for the perturbed magnetic field in a cold, inhomogeneous, and magnetized plasma with one ion species can be obtained from the Maxwell equations

[a]Scientific Centre, Institute for Nuclear Research Kyiv, Ukraine.

 © 2000 American Institute of Physics

Downloaded 01 Oct 2003 to 129.16.123.202. Redistribution subject to AIP license or copyright, see http://ojps.aip.org/pop/popcr.jsp

$$\nabla\times\mathbf{B}=\frac{4\pi}{c}\mathbf{j}, \tag{1}$$

$$\nabla\times\mathbf{E}=\frac{i\omega}{c}\mathbf{B}, \tag{2}$$

where it is assumed that the perturbed quantities X depend on time as $\exp(-i\omega t)$, ω is the wave frequency, $j_i=\sigma_{ij}E_j$, σ_{ij} is the conductivity tensor being related to the dielectric tensor ϵ_{ij} through $\epsilon_{ij}=\delta_{ij}+i4\pi\sigma_{ij}/\omega$.

Let us introduce the coordinates x^1, x^2, and x^3, where x^1 is a radial coordinate such that x^1 is constant on a flux surface, $x^2=\theta$ is the poloidal angle and $x^3=\varphi$ is the toroidal angle. The corresponding E_i and B_i are the co-variant components of $\mathbf{E}$ and $\mathbf{B}$. We assume vanishing parallel electric field $(E_3+E_2/q\simeq 0)$, where the safety factor is $q=d\Phi/d\Psi$, where Φ and Ψ are the toroidal and poloidal magnetic fluxes, respectively. Furthermore we assume a safety factor that is large enough $[q\gg(r/R)(E_\theta/E_\varphi)]$, so that $E_3\simeq 0$. This condition is satisfied for large aspect ratio, in the region of the interest: near the edge of the plasma.

If we furthermore assume toroidal variation as $X\propto\exp(-in\varphi)$, where n is the toroidal mode number, we can use Eq. (1) to express E_1 and E_2 in terms of B_3 as

$$E_1=\frac{c}{R^2\omega\epsilon_{12}(1+F_n)}\left[iR\frac{\partial B_3}{\partial r}-\sqrt{g}g^{22}\frac{\omega_{ci}}{\omega}\left(1-\frac{C_n}{\epsilon_{22}}\right)\frac{\partial B_3}{\partial\theta}\right], \tag{3}$$

$$E_2=\frac{c}{R^2\omega\epsilon_{12}(1+F_n)}\left[iR\frac{\partial B_3}{\partial\theta}+\sqrt{g}g^{11}\frac{\omega_{ci}}{\omega}\left(1-\frac{C_n}{\epsilon_{11}}\right)\frac{\partial B_3}{\partial r}\right], \tag{4}$$

where

$$F_n=\frac{gg^{11}g^{22}}{R^2}\frac{\epsilon_{11}\epsilon_{22}}{\epsilon_{12}^2}\left(1-\frac{C_n}{\epsilon_{11}}\right)\left(1-\frac{C_n}{\epsilon_{22}}\right), \tag{5}$$

$C_n=-(nc)^2/(R\omega)^2$, $g=\det g_{ij}$, g_{ij} is the metric tensor and R is the major radius of the torus. In the case of a plasma with elliptical cross section, the metric tensor is, cf. Ref. 8

$$\begin{aligned} g^{11}&=\kappa^{-2}\sin^2\theta+\cos^2\theta,\\ g^{22}&=(\sin^2\theta+\kappa^{-2}\cos^2\theta)/r^2,\\ g^{12}&=g^{21}=-(1-\kappa^{-2})\sin\theta\cos\theta/r,\\ \sqrt{g}&=\kappa rR, \end{aligned} \tag{6}$$

where κ is the ellipticity of the flux surface defined as the ratio of major and minor radius of the ellipse. We assume that κ is constant as a function of r.

In the frequency range $\omega_{ci}^2\ll\omega^2$ the dielectric tensor elements can be simplified to

$$\epsilon_{11}=\epsilon_{22}=-\frac{\omega_{pi}^2}{\omega^2},\quad \epsilon_{12}=-\epsilon_{21}=-i\frac{\omega_{pi}^2}{\omega\omega_{ci}}, \tag{7}$$

where ω_{pi} is the ion plasma frequency. This high-frequency limit is relevant to the harmonics $l\gtrsim 3$ of the ICE emission lines. Furthermore, using Eqs. (7), F_n defined by Eq. (5) can be rewritten as

$$F_n\simeq-\left(\frac{1+K_n}{l}\right)^2(1+\sin^2\theta\cos^2\theta(\kappa-\kappa^{-1})^2), \tag{8}$$

where l is the cyclotron harmonic number, $K_n=(v_An)^2/(\omega_{ci}R)^2$, and v_A is the Alfvén velocity. Note that for large safety factor q and high toroidal mode numbers n, the parallel wave number can be approximated as $k_\parallel\simeq n/R$ leading to $K_n\simeq(v_Ak_\parallel/\omega_{ci})^2$. Since $(1+K_n)^2\ll l^2$ for typical experimental conditions in tokamaks, F_n is negligible. Taking the third component of Eq. (2),

$$\frac{\partial E_2}{\partial r}-\frac{\partial E_1}{\partial\theta}=i\frac{\omega}{c}\frac{\sqrt{g}}{R^2}B_3 \tag{9}$$

and using Eqs. (3) and (4), we arrive at the following eigenmode equation for B_3:

$$\begin{aligned} &\frac{\partial}{\partial r}\left(\sqrt{g}g^{11}\frac{v_A^2}{c^2}(1+K_n)\right)\frac{\partial B_3}{\partial r}+\frac{\partial}{\partial\theta}\left(\sqrt{g}g^{22}\frac{v_A^2}{c^2}(1+K_n)\right)\frac{\partial B_3}{\partial\theta}\\ &\quad+\frac{\partial}{\partial\theta}\left(\frac{R}{\epsilon_{12}}\frac{\partial B_3}{\partial r}\right)-\frac{\partial}{\partial r}\left(\frac{R}{\epsilon_{12}}\frac{\partial B_3}{\partial\theta}\right)+\frac{\omega^2}{c^2}\sqrt{g}B_3=0, \end{aligned} \tag{10}$$

where $B_3\simeq RB_\parallel-B_2/q\simeq RB_\parallel$ is the toroidal component of the perturbed magnetic field.

Note that for circular cross section $(g^{11}=r^2g^{22}=1)$ and $B_3\propto\exp(im\theta)$, Eq. (10) reduces to the eigenmode equation considered in Refs. 3 and 4. For a noncircular cross section, in the large aspect ratio limit $(a\ll R)$, Eq. (10) can be simplified to

$$\begin{aligned} &\left[\frac{g^{11}}{rv_A^2}\frac{\partial}{\partial r}rv_A^2(1+K_n)\frac{\partial}{\partial r}+(1+K_n)\frac{\partial}{\partial\theta}g^{22}\frac{\partial}{\partial\theta}\right.\\ &\quad\left.+\frac{i}{r}\frac{n_i'}{n_i}\frac{\omega}{\omega_{ci}\kappa}\frac{\partial}{\partial\theta}+\frac{\omega^2}{v_A^2}\right]B_\parallel=0, \end{aligned} \tag{11}$$

where $n_i(r)$ is the density profile of the bulk ions and the prime denotes a radial derivative. Introducing

$$B_\parallel(r,\theta)=\hat{B}(r,\theta)e^{im(\theta+\epsilon_0\sin\theta)} \tag{12}$$

with $\epsilon_0=a/(R_0+a)$, we obtain the following equation:

$$\begin{aligned} &\left[\frac{g^{11}}{rv_A^2}\frac{\partial}{\partial r}rv_A^2(1+K_n)\frac{\partial}{\partial r}+g^{22}(1+K_n)\frac{\partial^2}{\partial\theta^2}\right]\hat{B}-V(r,\theta)\hat{B}\\ &\quad+i\left[\frac{1}{r}\frac{\omega}{\kappa\omega_{ci}}\frac{n_i'}{n_i}+2mg^{22}(1+K_n)(1+\epsilon_0\cos\theta)\right]\frac{\partial\hat{B}}{\partial\theta}=0 \end{aligned} \tag{13}$$

with the potential

$$\begin{aligned} V(r,\theta)&=(1+K_n)m^2(1+\epsilon_0\cos\theta)^2g^{22}-\frac{\omega^2}{v_A^2}\\ &\quad+\frac{m\omega n_i'}{r\kappa\omega_{ci}n^i}(1+\epsilon_0\cos\theta)+im(1+K_n)\\ &\quad\times\left(g^{22}\epsilon_0\sin\theta-(1+\epsilon_0\cos\theta)\frac{\partial g^{22}}{\partial\theta}\right). \end{aligned} \tag{14}$$

In the above equation, toroidal effects have been included in v_A and ω_{ci} through the poloidal dependence of the equilib-

Downloaded 01 Oct 2003 to 129.16.123.202. Redistribution subject to AIP license or copyright, see http://ojps.aip.org/pop/popcr.jsp

rium magnetic field $B=B_0/(1+\epsilon\cos\theta)$. Thus, $v_A(r)=\hat{v}_A(r)/(1+\epsilon\cos\theta)$ and $\omega_{ci}=\hat{\omega}_{ci}/(1+\epsilon\cos\theta)$, where $\epsilon=r/R$ and B_0 is the magnetic field at the plasma center. The term proportional to n_i'/n_i originates from the Hall term, which has been included in the infinite aspect ratio limit in Refs. 3, 4 and 7. Note that this term breaks the poloidal symmetry even when ϵ is negligibly small.

In deriving Eq. (13), we have neglected the mode coupling associated with the ellipticity, cf. Ref. 7. This approximation is justified in the limit when the ellipticity is not too large, i.e.,

$$\frac{\kappa^2-1}{2(\kappa^2+1)}\ll 1 \tag{15}$$

which is well satisfied in most of cases of interest.

III. VARIATIONAL ANALYSIS

For real $\hat{B}$, the Lagrangian corresponding to Eq. (13) is given by

$$L=(\partial\hat{B}/\partial r)^2+1/r^2(\partial\hat{B}/\partial\theta)^2+H(r,\theta)\hat{B}^2, \tag{16}$$

where $H(r,\theta,\omega)=\mathrm{Re}[V(r,\theta,\omega)]$. Assuming now an ansatz function of the form

$$\hat{B}(r,\theta)=B_0\exp\left(-\frac{(r-r_0)^2}{2\Delta^2}\right)\exp\left(-\frac{(\theta-\theta_0)^2}{2\eta^2}\right) \tag{17}$$

the variational principle $\delta\int dr\,d\theta\,L(r_0,\Delta,\theta_0,\eta)=0$ determines the localization radius r_0, the radial localization width Δ, the localization angle θ_0 and the poloidal localization width η. The variations with respect to r_0 and θ_0 imply that

$$\left.\frac{\partial H}{\partial r}\right|_{r_0,\theta_0}=0, \tag{18}$$

$$\left.\frac{\partial H}{\partial\theta}\right|_{r_0,\theta_0}=0, \tag{19}$$

where we assumed that $\partial H/\partial r$ and $\partial H/\partial\theta$ are slowly varying in the vicinity of r_0 and θ_0. To find the rest of the parameters we expand $H(r,\theta,\omega)$ around r_0 and θ_0. Then, the variations with respect to B_0^2, Δ and η give the following set of equations:

$$\Delta^4=\left.\frac{2}{\partial^2H/\partial r^2}\right|_{r_0,\theta_0}, \tag{20}$$

$$\eta^4=\left.\frac{2}{r_0^2\partial^2H/\partial\theta^2}\right|_{r_0,\theta_0}, \tag{21}$$

$$H(r_0,\theta_0,\omega)+\frac{2}{\Delta^2}\left(1+\frac{\Delta^2}{r_0^2\eta^2}\right)=0. \tag{22}$$

Introducing $\omega=\omega_0+\delta\omega$, $|\delta\omega|\ll\omega_0$, Eq. (22) leads to

$$H(r_0,\theta_0,\omega_0)=0, \tag{23}$$

$$\delta\omega=-\frac{2}{\Delta^2}\left(1+\frac{\Delta^2}{r_0^2\eta^2}\right)\Big/\left.\frac{\partial H}{\partial\omega}\right|_{r_0,\theta_0}. \tag{24}$$

Equations (18), (19), and (23) determine the eigenmode frequency ω_0 and localization radius r_0 and angle θ_0.

In the general case Eqs. (18), (19), and (23) have to be solved numerically. The conditions for localized solutions are $\partial^2H/\partial\theta^2>0$ and $\partial^2H/\partial r^2>0$. In the large aspect ratio case ($\epsilon\ll 1$), we can neglect the correction terms of $O(\epsilon)$ and obtain $\partial H/\partial\theta=\sin 2\theta(1+K_n)m^2(1-\kappa^{-2})/r^2=0$, which together with the condition $\partial^2H/\partial\theta^2>0$ gives $\theta_0=0$ or π, in agreement with the result of Ref. 6. Thus, the ellipticity should not affect the poloidal localization angle: i.e., $\theta_0=0$ or $\theta_0=\pi$ are independent of κ.

The eigenmode frequency is given by

$$\omega_0=\left.\frac{|m|\hat{v}_A}{\kappa r}\left\{\frac{\sigma_m\hat{v}_An_i'}{2\hat{\omega}_{ci}n_i}+\left[(1+K_n)+\left(\frac{\hat{v}_An_i'}{2\hat{\omega}_{ci}n_i}\right)^2\right]^{1/2}\right\}\right|_{r=r_0} \tag{25}$$

and the localization radius r_0 is determined by the equation

$$2+r\frac{n_i'}{n_i}-\sigma_m\frac{\hat{v}_A}{\sqrt{(1+K_n)}\,\hat{\omega}_{ci}}\left(\frac{rn_i'}{n_i}\right)'\left(1-\frac{n_i'}{n_i}\frac{2+rn_i'/n_i}{(rn_i'/n_i)'}\right)^{1/2}=0, \tag{26}$$

where σ_m denotes the sign of the poloidal wave number m. Note that Eqs. (25) and (26) are valid only in the large aspect ratio limit. A more general numerical result of Eqs. (18) and (19) is presented in Sec. III A for the finite aspect ratio case. Also these numerical calculations lead to the same localization angles $\theta=0$ or $\theta=\pi$, but the eigenfrequency and localization radius will be shifted. These results are in agreement with those of Refs. 3 and 4 for a circular cross section ($\kappa=1$) and vanishing parallel wave number ($K_n=0$). For the poloidal localization width, we find

$$\eta^2=(\Delta/r_0)\sqrt{2(1+\epsilon_0)/\epsilon_0} \tag{27}$$

in agreement with Ref. 6. Thus, the poloidal localization width is a function of the aspect ratio. For the infinite aspect ratio (cylindrical) case there is no poloidal variation and the lower the aspect ratio, the stronger the poloidal localization.

A. Asymmetry in the sign of the poloidal mode number

As noted in previous work,[3,4,7] Eq. (26) always have solutions for negative poloidal mode numbers $m<0$. Thus localized solutions can be expected for $m<0$. For $m>0$ the situation is more complex as being sensitive to the ion density profile, the ellipticity and the toroidal mode number.

Here we use the density profile $n_i(r)=n(0)(1-(r/a)^p)^\nu$, with different combinations of ν and p. The density profile with $\nu=0.5$ and $p=2$ fits the experimental profiles rather well in the region $0.6<r/a<0.8$. However, this choice of density profile leads to $n_i'\to\infty$ for $r\to a$ which is unrealistic. To investigate the effect of the density profiles, we have also solved Eq. (18) numerically (and examined the eigenmode behavior in the next section) for a profile with $\nu=1$ and $p=3$ that provide an acceptable characteristic in the region $r/a\geqslant 0.7$ and has a finite derivative at the edge.

For the density profile with the parameters $\nu=0.5$ and $p=2$, a circular cross section and infinite aspect ratio, the

Downloaded 01 Oct 2003 to 129.16.123.202. Redistribution subject to AIP license or copyright, see http://ojps.aip.org/pop/popcr.jsp

obtained results agree with those of Refs. 3 and 4: the presence of solutions of Eq. (18) depends on the sign of the poloidal mode number m. For $m<0$, Eq. (18) always possesses solutions, which means that we can expect localized solutions to the eigenmode equation. For $m>0$, and typical experimental parameters, Eq. (18) does not have any solution and we expect that the solution to the eigenmode equation will not be localized. The numerical calculations presented in the following section show solutions that are not decaying at the plasma edge, because the gradient of the perturbed magnetic field does not vanish, even if the field itself does.

However, for elliptic cross section [$\kappa=1.6$ for Joint European Torus (JET)], Eq. (18) can have solutions for both signs of m, and therefore localized eigenmode solutions can be expected for both signs of m, when the plasma density exceeds a critical magnitude at the outer plasma edge or equivalently when the ratio $d_i=v_A/\omega_{ci}$ evaluated near the edge is lower than a critical magnitude $d_i^{\rm crit}$. This result is in agreement with Refs. 3, 4, and 7, where the existence of the localized solutions has been investigated in the limit of infinite aspect ratio. If the density profile is assumed to be of the form $n(r)\propto(1-(r/a)^p)^\nu$, the critical edge density is related to a critical central density. For simplicity we will use the fixed density profile described above, and calculate the critical parameter d_i evaluated at the center, but we should keep in mind, that for the localization of the wave, the conditions at the edge are important and in reality these might not be related to the ones at the center by the assumed simple expression.

In the toroidal case with $R_0/a=3$, we have solved Eq. (18) numerically, using the parameters: $a=115\,\text{cm}$, $R=321\,\text{cm}$, $\hat{\omega}_{ci}=10^8\,\text{s}^{-1}$ and $\kappa=1.6$. For vanishing parallel wave number $k_\parallel\simeq n/R=0$ and localization angle $\theta_0=0$, the density profile with the parameters $\nu=1$ and $p=3$ corresponds to the critical parameter $d_{i0}^{\rm crit}=3.4$, while the density profile used with the parameters $\nu=0.5$ and $p=2$, used in Ref. 3, gives a somewhat lower critical parameter: $d_{i0}^{\rm crit}=2.7$. Note that both these values are lower than the estimated d_{i0} in the center of the plasma in the JET preliminary tritium experiments (PTE) [$d_{i0}=7.1$, (Ref. 9)]. Thus, according to this simplified analysis, for the JET PTE experiment, only eigenmodes with negative m are expected to be localized. However, including finite $k_\parallel$ corrections raises the d_{i0} threshold and leads to a different conclusion.

Let us illustrate the effect of finite $k_\parallel$ with some examples. For the density parameters $\nu=1$ and $p=3$ and toroidal mode number $n=10$ (corresponding to $k_\parallel\simeq 3\,\text{m}^{-1}$) we obtain $d_{i0}<d_{i0}^{\rm crit}=3.8$. This is a slight increase from the value corresponding to $n=0$ ($d_{i0}^{\rm crit}=3.4$). However, for the higher toroidal mode number, $n=20$ ($k_\parallel\simeq 6\,\text{m}^{-1}$), there is a very dramatic increase, and the restriction on d_{i0} is completely removed (for the experimental parameters of interest). In other words, localized eigenmodes exist for both signs of m without any restriction on the plasma density. Note, that for circular cross section ($\kappa=1$), there is still a restriction on d_{i0} even for $n=20$, and it disappears only when both finite $k_\parallel$ corrections and the ellipticity ($\kappa\neq 1$) are taken into account at the same time. For the density profile with $\nu=0.5$ and $p=2$, there is a restriction even for $n=20$ and $\kappa=1.6$, namely, $d_{i0}<d_{i0}^{\rm crit}=3.6$. The critical parameters corresponding to the localization angle $\theta_0=\pi$ are generally slightly higher those for $\theta_0=0$. In the present paper we concentrate mainly on the poloidal localization around $\theta_0=0$, since the observed ICE usually originates from the outer midplane edge, as a result of the fact that fast ions driving the instability has a highly anisotropic velocity distribution in that region. However, we expect similar solutions for $\theta_0=\pi$. Figure 1 shows the normalized localization radius, obtained from solving Eq. (18), as a function of the parameter $d_{i0}=v_{A0}/\omega_{ci}$. Note that in three of the cases there are no solutions for the radius of localization above a critical d_{i0}. This d_{i0} corresponds to a critical edge density above which no solutions exist. However, for the density parameters $\nu=1$, $p=3$, and $n=20$ (dotted line) Eq. (18) has solutions for all d_{i0}, that is for all edge densities.

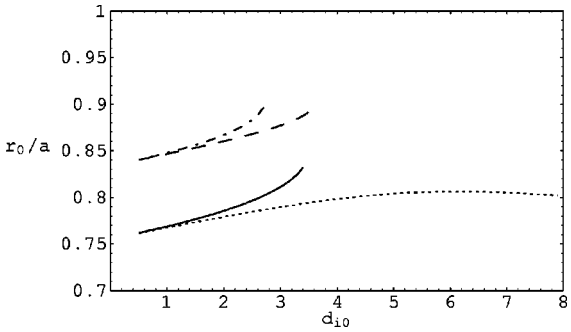

FIG. 1. Radius of localization as a function of the parameter $d_{i0}=v_{A0}/\omega_{ci}$, for poloidal mode number $m=25$, aspect ratio $R_0/a=3$ and ellipticity $\kappa=1.6$: $\nu=1$, $p=3$, $n=0$ (solid); $\nu=1$, $p=3$, $n=20$ (dotted); $\nu=0.5$, $p=2$, $n=0$ (dash–dotted); $\nu=0.5$, $p=2$, $n=20$ (dashed).

In summary, including finite $k_\parallel$ eliminates the restriction on the plasma density at the outer edge, and leads to localized solutions for both signs of the poloidal wave number, in the case of the $R_0/a=3$ aspect ratio, elliptic cross section tokamak. For $n<20$, localized solutions only exist when the plasma density is higher than a critical value at the outer edge. This critical plasma density varies with the ellipticity, aspect ratio, and the density profile. The importance of the finite parallel wave number has been noted also in Ref. 4.

B. ICE doublet lines

In the JET preliminary tritium experiment the ICE emission spectral lines were doublets, whereas in the Tokamak Fusion Test Reactor (TFTR) experiments only singlet ICE lines were observed. According to the theoretical analysis in Ref. 10, the doublet lines are the result of the destabilization of waves with both positive and negative poloidal mode numbers, m. Therefore the localization condition of waves with both signs of m is important for the interpretation of the experimental data.

In the limit of circular cross section and infinite aspect ratio, Ref. 3 showed that if $d_i<d_i^{\rm crit}$, edge localized FME can only exist if the mode poloidal phase velocity has the same direction as the ion cyclotron motion, or in other words, modes with only one sign of poloidal mode number m can exist. For the JET experimental parameters, the calcu-

Downloaded 01 Oct 2003 to 129.16.123.202. Redistribution subject to AIP license or copyright, see http://ojps.aip.org/pop/popcr.jsp

lated critical parameter $d_i^{\rm crit}$ was too low, leading to the conclusion that modes with only one sign of m could exist. However, modes with both signs of m could exist in TFTR, mainly because the density was much higher there, and $d_i^{\rm crit}$ is inversely proportional to the square root of the density.

Including the ellipticity, but still in the cylindrical limit, the analysis of Ref. 7 led to a significant modification of the expression of $d_i^{\rm crit}$ and a different conclusion, i.e., comparison with experimental data showed that the condition $d_i < d_i^{\rm crit}$ was possible to satisfy in the JET experiment (depending on the chosen density profile), while it was not satisfied in the TFTR experiment. This result contradicted the conclusion of Ref. 3, and the main reason was the sensitive dependence of $d_i^{\rm crit}$ on the ellipticity, as we have also seen in the preceding subsection in the 2D case.

Our analysis in the preceding subsection confirms the result of Ref. 7, in the sense that it predicts the existence of localized waves with both signs of m in a finite aspect ratio tokamak with elliptic cross section, like JET. In the infinite aspect ratio case, our results coincide with those of both Ref. 3 for circular cross section and Ref. 7 for elliptic cross section. The critical parameters calculated in the preceding subsection are valid for the ellipticity $\kappa = 1.6$, and are applicable to the JET experiment. For a circular cross section tokamak, as in TFTR, the critical parameters are considerably lower. This is the main reason for the disagreement between our results and those of Ref. 3 regarding the existence of localized solutions with both signs of m for JET.

In the TFTR experiment, the observed ICE emission was characterized by singlet lines. However, that observation does not necessarily mean that FME with only one sign of m are localized in the emitting region, because, as we showed in Ref. 11, the doublet width in TFTR is predicted to be too small to be discernible in experiments. Moreover, the analysis of the TFTR ICE data is difficult, due to the lack of a complete data set from the shots, where the ICE has been observed. Therefore, in this case the density profile has to be inferred from several similar shots. Furthermore, the choice of the ion density profile is difficult, since it can change considerably during one experiment, see for instance the TFTR supershot experiment,[12] where the density profile is peaked during the NBI and flattens and is reduced with about a factor 2, after the termination of NBI.

IV. NUMERICAL ANALYSIS

The eigenvalue equation (13) is solved numerically, to investigate how the aspect ratio, R/a, the ion density profile, $n_i(r)$, the poloidal mode number, m, the toroidal mode number, n, and the ellipticity, κ, affect the eigenmode localization properties. Equation (13) is a partial differential equation in radius r and poloidal angle θ with periodic boundary conditions in θ and vanishing field solutions, $\hat{B}(r,\theta)=0$ and $\partial\hat{B}/\partial r = 0$, at $r=0$ as well as at the edge of the plasma $r=a$. The solution is obtained by discretizing the PDE in the θ direction to a system of k coupled ordinary differential equations and by solving this system with the shooting method. To avoid numerical difficulties associated with the zero boundary conditions we shoot toward the boundaries from a point r_m where the field is nonvanishing. We minimize the L^2 error at the boundaries with respect to the eigenfrequency ω_0 and the values of $\hat{B}(r_m)$ and $\partial\hat{B}/\partial r(r_m)$ at a chosen point r_m. Since $\hat{B}$ is complex, this amounts to a $4k$ dimensional minimization. In the limit of infinite aspect ratio, there is no poloidal variation, and the minimization will be only four dimensional. However, for lower aspect ratio, we need to take into account the poloidal variation, and to make the calculations numerically feasible we have restricted our analysis to the real part of the equation, thereby reducing the minimization to $2k$ dimensions. According to Eq. (12), the definition of $\hat{B}$ is such that the phase variation of the magnetic field is captured in the exponential $e^{im(\theta+\epsilon_0\sin\theta)}$. The form of the exponential has been found in Ref. 1 by using a combined expansion in powers of the two smallness parameters m^{-1} and the inverse aspect ratio ϵ_0. Assuming that the phase variation of $\hat{B}$ is negligible it follows that the absolute value of $\hat{B}$ is proportional to the real part of $\hat{B}$. Thus the real part of the equation gives a good approximation of the form of the absolute value of magnetic field. The validity of this assumption has been confirmed numerically in the limit of infinite aspect ratio.

The radial variation of the eigenmodes is presented by showing the intersection of the solution surface with the planes $\theta = 2\pi j/k$, for $j=0,1,\ldots,k-1$. The discretization parameter is chosen to $k=11$. The poloidal variation is presented by showing contour plots of the real part of the perturbed magnetic field $\hat{B}$. We have studied differences in the mode behavior between

(a) the cylindrical ($R_0/a=\infty$) vs the toroidal ($R_0/a=3$) case;
(b) density profiles with $\nu=0.5$ and $p=2$, and $\nu=1$ and $p=3$;
(c) circular and elliptic cross sections ($\kappa=1$ and $\kappa=1.6$);
(d) different signs of the poloidal mode number, m;
(e) vanishing and finite toroidal mode number, n.

The calculations were performed for $a=115$ cm, $v_{A0}=7.5\times10^8$ cm/s and $\hat{\omega}_{ci}=10^8$ s^{-1}. These parameters are characteristic of the JET plasma experiment where superthermal ICE has been observed.

A. Circular cross section

The case of circular cross section has been thoroughly examined both numerically and analytically.[1–6] For completeness, we have repeated the analysis and compared our results with the previously published ones.

In the cylindrical case ($R_0/a=\infty$), the eigenmodes are localized radially in a ring close to the plasma edge. The eigenfrequencies for a given poloidal mode number m are regularly spaced with a frequency step of about $0.25\,\omega_{ci}$. The radial width of the eigenmodes is inversely proportional to m, and it increases with the eigenfrequency. Our results are in agreement with previous works, see, e.g., Ref. 4. Figure 2 shows the radial variation of the first three eigenmodes for the density profile with $\nu=0.5$, $p=2$, and $m=-25$.

Downloaded 01 Oct 2003 to 129.16.123.202. Redistribution subject to AIP license or copyright, see http://ojps.aip.org/pop/popcr.jsp

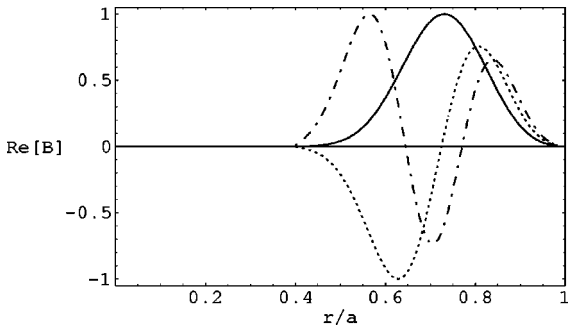

FIG. 2. Radial variation of the real part of the magnetic field $\hat{B}$ for $R_0/a=\infty$, density profile $n_i(r)=n(0)(1-(r/a)^2)^{0.5}$ and circular cross section. The eigenfrequencies are $\omega=3\,\omega_c$ (solid), $\omega=3.25\,\omega_c$ (dotted), and $\omega=3.5\,\omega_c$ (dash–dotted).

There is no poloidal variation, since the θ dependent term vanishes in the eigenmode equation as $R\to\infty$. The imaginary part of the eigenmodes is at least two orders of magnitude smaller than the real part and exhibits a similar behavior as the real part.

In the toroidal case ($R_0/a=3$), the main difference compared to the cylindrical case is the poloidal localization of the eigenmodes around $\theta_0=0$. The radial and poloidal localization width is consistent with the predictions of the variational analysis. Also in this case, the eigenmodes are regularly spaced, and the radial variation is not too different from the cylindrical case, but in this case the intersection curves (with the planes $\theta=2\pi j/k$, for $j=0,1,\ldots,k-1$) do not lie on top of each other as they did in the cylindrical case since the eigenfunction is not constant poloidally. Figures 3 and 4 show the poloidal and radial variation of the eigenmodes for the parameters $\nu=0.5$, $p=2$, $m=\pm 25$. As expected, the positive poloidal mode number $m=25$ leads to eigenmodes that are not decaying at the edge [see Fig. 4(b) and the finite derivative of $\hat{B}$ at $r=a$], i.e., there are no solutions to the eigenvalue problem that satisfy the boundary condition $\partial\hat{B}/\partial r=0$ at $r=a$. The eigenfrequency is somewhat shifted as compared to the cylindrical case, i.e., $\omega=3\,\omega_{ci}$ for $R_0/a=\infty$ and $\omega=3.1\,\omega_{ci}$ for $R_0/a=3$.

The solutions of the eigenvalue problem have been compared for the density profile parameters $\nu=0.5$, $p=2$ and $\nu=1$, $p=3$. For a circular cross section, the resulting eigenmode behavior is qualitatively similar for the two density profiles. The only difference is that the radius of localization is shifted towards the plasma center. This shift in radius is sustained for a wide range of plasma parameters, and it can be also seen in Fig. 1, where the localization radius is showed for an elliptic cross section and aspect ratio $R_0/a=3$ as a function of the parameter $d_{i0}=v_{A0}/\omega_{ci}$.

B. Elliptical cross section

We now proceed to the calculations performed for elliptic cross section ($\kappa=1.6$), keeping the rest of the parameters the same as in the case of the circular cross section ($\kappa=1$). Calculations for $1<\kappa<1.6$ has also been carried out

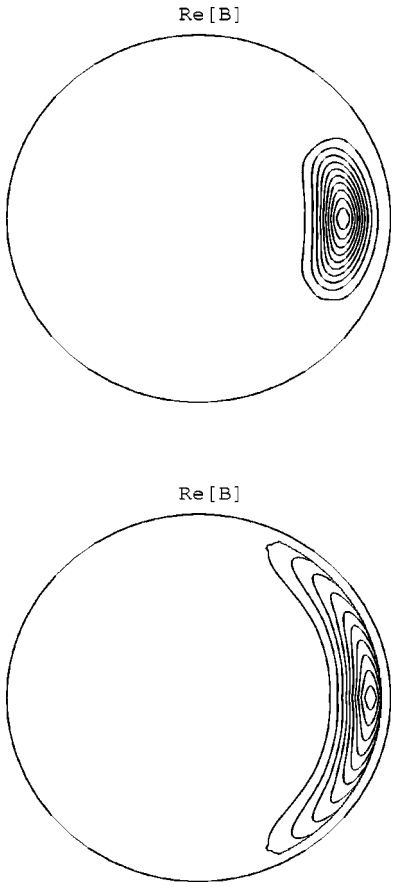

FIG. 3. Poloidal variation of the real part of the magnetic field $\hat{B}$ for aspect ratio $R_0/a=3$, density profile $n_i(r)=n(0)(1-(r/a)^2)^{0.5}$, circular cross section, $n=0$ and (a) $\omega=3.1\,\omega_{ci}$, $m=-25$; (b) $\omega=2.4\,\omega_{ci}$, $m=25$.

and the results change continuously and monotonously between the two extremes. Here, we only present the results for $\kappa=1.6$.

In the cylindrical case ($R_0/a=\infty$), the resulting eigenmode behavior is qualitatively the same as for $\kappa=1$, and only the eigenmode frequency is affected. For the density parameters $\nu=0.5$ and $p=2$, the eigenmode frequency is shifted down from $\omega=3\,\omega_{ci}$ ($\kappa=1$) to $\omega=2.45\,\omega_{ci}$ ($\kappa=1.6$). Also for the density parameters $\nu=1$ and $p=3$, the shift in the eigenfrequency is about the same: from $\omega=3.27\,\omega_{ci}$ for $\kappa=1$ to $\omega=2.67\omega_{ci}$ for $\kappa=1.6$. The change in the ellipticity does not affect the radius of localization considerably.

In the toroidal case ($R_0/a=3$), the inclusion of the ellipticity affects both the eigenvalues and the mode structure. For each order of radial eigenmode, different poloidal eigenmodes may exist. The first order eigenmode in both r and θ [denoted by (1,1), with the two numbers corresponding to the radial and poloidal order of the eigenmodes, respectively] looks similar to the one obtained for $\kappa=1$. In this case only the eigenvalues differ. For the second order (1,2) eigenmode, additional poloidal peaks appear at $\theta\neq 0$. However, the radial mode structure and localization radius is similar to that obtained for (1,1) and for a circular cross section. Figure 5 shows the poloidal variations of the eigenmode (1,1) and (1,2) for the ellipticity $\kappa=1.6$ (JET), toroidal wave number

Downloaded 01 Oct 2003 to 129.16.123.202. Redistribution subject to AIP license or copyright, see http://ojps.aip.org/pop/popcr.jsp

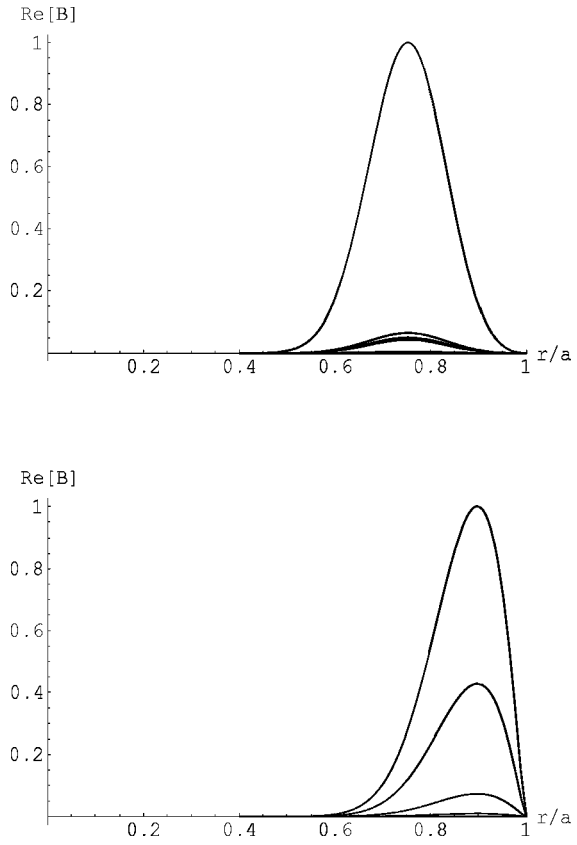

FIG. 4. Radial variation of the real part of the magnetic field $\hat{B}$ for $\theta = 2\pi j/11$, $j = 0,1,\ldots,10$ and for the same parameters as in Fig. 3.

$n = 20$ and density parameters $\nu = 0.5$ and $p = 2$.

For the density parameters $\nu = 1$ and $p = 3$, the qualitative behavior is similar to the $\nu = 0.5$ and $p = 2$ case. Also here, for each order of radial eigenmode we find different poloidal eigenmodes, and the lowest order poloidal eigenmode is well localized around $\theta = 0$. Also in the toroidal case, the inclusion of the ellipticity affects the eigenfrequency and introduces a frequency shift. For example, for

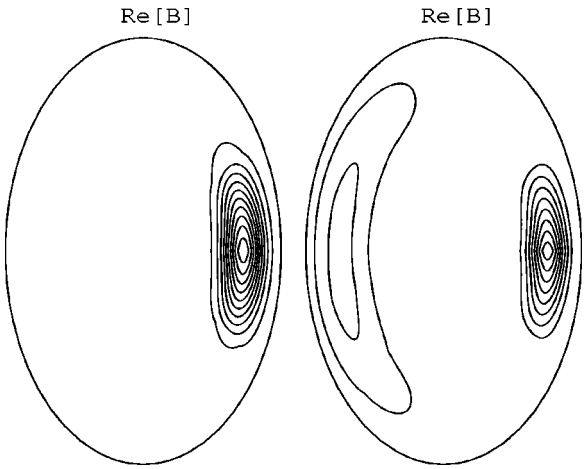

FIG. 5. Poloidal variation of the real part of the magnetic field $\hat{B}$ for aspect ratio $R_0/a = 3$, density profile $n_i(r) = n(0)(1-(r/a)^2)^{0.5}$, ellipticity $\kappa = 1.6$, $n = 20$ and $m = -25$. The eigenmode orders and eigenfrequencies are (left) (1,1) and $\omega = 2.35\,\omega_{ci}$ and (right) (2,1) and $\omega = 2.23\,\omega_{ci}$.

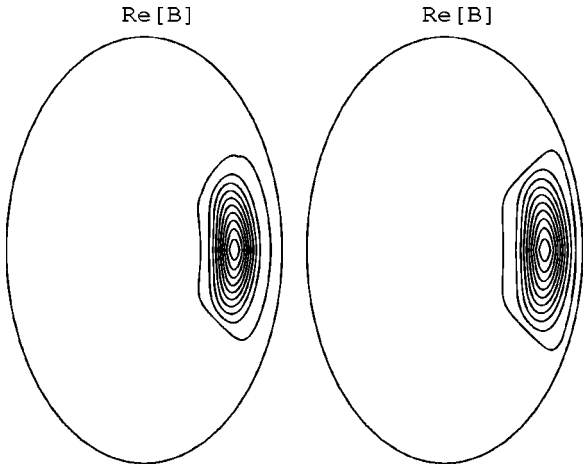

FIG. 6. Poloidal variation of the real part of the magnetic field $\hat{B}$ for aspect ratio $R_0/a = 3$, density profile $n_i(r) = n(0)(1-(r/a)^3)$, $\kappa = 1.6$, $n = 20$ and (left) $m = -25$, $\omega = 2.5\,\omega_{ci}$, and (right) $m = 25$, $\omega = 2.1\,\omega_{ci}$.

$m = -25$ the eigenfrequency changes from $\omega = 3.4\,\omega_{ci}$ for $\kappa = 1$, $n = 0$ to $\omega = 3\,\omega_{ci}$ for $\kappa = 1.6$, $n = 0$. Furthermore, the inclusion of the finite n introduces another frequency shift to $\omega = 2.5\,\omega_{ci}$ for $\kappa = 1.6$, $n = 20$.

We have also compared the mode structure for different signs of m and the existence of localized solutions for $m > 0$. For $n = 0$, the difference for the different signs of m is sustained, and the gradient of the field does not vanish at the plasma edge for $m > 0$, unless the central Alfvén velocity is lower than the critical value. This critical value is higher for the density profile with the density parameters $\nu = 1$, $p = 3$ than for the profile with the parameters $\nu = 0.5$, $p = 2$.

Keeping finite toroidal mode number leads to localized solutions for both signs of m. For $n = 0$, the eigenmode is not decaying at the edge, which is in agreement with the variational analysis in the previous section. For $n = 20$, the eigenmode is localized both radially and poloidally. Figure 6 shows the poloidal variation of the eigenmodes for the aspect ratio $R_0/a = 3$ and $m = \pm 25$, $\kappa = 1.6$, and $n = 20$. Note the localized poloidal structure for both signs of poloidal mode number. Thus the numerical results confirm the conclusion of the variational analysis, and show that both finite $k_\parallel$ and ellipticity effects are needed for the existence of localized waves for $m > 0$.

V. CONCLUSION

We have examined the 2D localization of the fast magnetoacoustic eigenmodes using numerical and analytical methods. The present analysis shows, that the FME are edge-localized in the radial direction. In the toroidal case (aspect ratio $R_0/a = 3$), the eigenmodes are localized also poloidally around $\theta \simeq 0$. However, the inclusion of the ellipticity leads to higher order solutions that have a more extended poloidal mode structure, but the lowest order solution is still well-localized. The numerical results show that the different radial eigenmodes are regularly spaced and both the width of the mode and the eigenmode frequency are in good agreement with the analytical predictions.

Downloaded 01 Oct 2003 to 129.16.123.202. Redistribution subject to AIP license or copyright, see http://ojps.aip.org/pop/popcr.jsp

The density profile has a strong influence on the eigenmode frequency and the localization radius. Moreover, for certain choices of the ion density profile, the symmetry in the sign of the poloidal mode number m is broken and for $m > 0$ the eigensolutions are not decaying at the plasma edge. This important symmetry breaking is caused by the Hall term (corresponding in our analysis to the off-diagonal elements of the dielectric tensor), and has been pointed out earlier in Ref. 3. Since different plasma experiments can have very different density profiles, the mode localization radius and the eigenmode frequency can be different. The eigenmode frequency is sensitive to changing the ellipticity, while the mode localization radius and the mode width are not affected considerably.

For relating with the ICE experimental data, apart from wave localization, also the resonance condition needs to be satisfied and a positive growth rate has to be found. These issues are out of the scope of this paper and are partly dealt with in Refs. 10 and 11. In these works, the growth rate was found to be maximum for $k_{\|} \simeq 0$. However, positive growth rates can be found also for finite $k_{\|}$ but these effects will modify the dispersion relation and give rise to a shift in the real part of the frequency.

ACKNOWLEDGMENTS

The authors thank Patrik Jansson for numerical advice. This work was supported by the European Community under an association contract between Euratom and Sweden.

[1] B. Coppi, S. Cowley, R. Kulsrud, P. Detragiache, and F. Pegoraro, Phys. Fluids **29**, 4060 (1986).
[2] B. Coppi, Phys. Lett. A **A172**, 439 (1993).
[3] B. Coppi, G. Penn, and C. Riconda, Ann. Phys. (N.Y.) **261**, 117 (1997).
[4] G. Penn, C. Riconda, and F. Rubini, Phys. Plasmas **5**, 2513 (1998).
[5] N. N. Gorelenkov and C. Z. Cheng, Phys. Plasmas **6**, 1961 (1995).
[6] N. N. Gorelenkov and C. Z. Cheng, Nucl. Fusion **35**, 1743 (1995).
[7] Ya. I. Kolesnichenko, T. Fülöp, M. Lisak, and D. Anderson, Nucl. Fusion **38**, 1871 (1998).
[8] Ya. I. Kolesnichenko, V. V. Parail, and G. V. Pereverzev, *Reviews of Plasma Physics* (Consultants Bureau, New York (1992), Vol. 17, p.l.
[9] G. A. Cottrell *et al.*, Nucl. Fusion **33**, 1365 (1993).
[10] T. Fülöp, Ya. I. Kolesnichenko, M. Lisak, and D. Anderson, Nucl. Fusion **37**, 1281 (1997).
[11] T. Fülöp and M. Lisak, Nucl. Fusion **38**, 761 (1998).
[12] R. V. Budny *et al.*, Nucl. Fusion **32**, 429 (1992).

Downloaded 01 Oct 2003 to 129.16.123.202. Redistribution subject to AIP license or copyright, see http://ojps.aip.org/pop/popcr.jsp